Title
Effect of heating/cooling dynamics in the hysteresis loop and tunable IR emissivity of VO2 thin films.

Journal
Optics Express, 28(26)

ISSN
1094-4087

Authors
Larciprete, Maria Cristina
Centini, Marco
Paoloni, Stefano
et al.

Publication Date
2020-12-21

DOI
10.1364/oe.411556

Peer reviewed

Research Article | Vol. 28, No. 26 / 21 December 2020 / Optics Express 39203
Optics EXPRESS

Effect of heating/cooling dynamics in the hysteresis loop and tunable IR emissivity of VO_2 thin films

MARIA CRISTINA LARCIPRETE,[1,*] MARCO CENTINI,[1] STEFANO PAOLONI,[2] SINA A. DERESHGI,[3] KECHAO TANG,[4] JUNQIAO WU,[4,5] AND KORAY AYDIN[3]

[1]*Dipartimento di Scienze di Base ed Applicate per l'Ingegneria, Sapienza Università di Roma, Via Antonio Scarpa 16, 00161 Rome, Italy*
[2]*Dipartimento di Ingegneria Industriale, Università degli Studi di Roma Tor Vergata, Via del Politecnico 1, 00133 Rome, Italy*
[3]*Department of Electrical and Computer Engineering, Northwestern University, Evanston, Illinois 60208, USA*
[4]*Department of Materials Science and Engineering, University of California, Berkeley, California 94720, USA*
[5]*Materials Sciences Division, Lawrence Berkeley National Laboratory, Berkeley, California 94720, USA*
[*]*mariacristina.larciprete@uniroma1.it*

Abstract: We experimentally investigate the semiconductor-to-metal transition (SMT) in vanadium dioxide thin films using an infrared thermographic technique. During the semiconductor to metal phase change process, VO_2 optical properties dynamically change and infrared emission undergoes a hysteresis loop due to differences between heating and cooling stages. The shape of the hysteresis loop was accurately monitored under different dynamic heating/cooling rates. In order to quantify and understand the effects of different rates, we used a numerical modelling approach in which a VO_2 thin layer was modeled as metamaterial. The main experimental findings are interpreted assuming that both the rate of formation and shape of metallic inclusions are tuned with the heating/cooling rate. The structural transition from monoclinic to tetragonal phases is the main mechanism for controlling the global properties of the phase transition. However, our experimental results reveal that the dynamics of the heating/cooling process can become a useful parameter for further tuning options and lays out a macroscopic optical sensing scheme for the microscopic phase change dynamics of VO_2. Our study sheds light on phase-transition dynamics and their effect on the infrared emission spectra of VO_2 thin films, therefore enabling the heating/cooling rate to be an additional parameter to control infrared emission characteristics of thermal emitters. The hysteresis loop represents the phase coexistence region, thus being of fundamental importance for several applications, such as the operation of radiative thermal logic elements based on phase transition materials. For such applications, the phase transition region is shifted for heating and cooling processes. We also show that, depending on the way the phase change elements are heated, the temperature operation range will be slightly modified.

1. Introduction

Thermochromic materials offer a drastic phase transition around their critical temperature (T_c), where significant optical, electrical and magnetic changes take place. Among several thermochromic materials such as niobium dioxide (NbO_2), vanadium sesquioxide (V_2O_3) [1], VO_2 undergoes a lattice transition from monoclinic (insulating) phase into a tetragonal (metallic) phase [2,3]. The low phase transition temperature, $T_c = 341$ K (68°C) along with the possibility of tuning it using different dopants fraction makes VO_2 is extensively employed. The significant changes due to lattice phase transition in spectral properties of VO_2 in both the IR [4] and THz

#411556 https://doi.org/10.1364/OE.411556
Journal © 2020 Received 2 Oct 2020; revised 11 Nov 2020; accepted 12 Nov 2020; published 11 Dec 2020

Optics EXPRESS

ranges [5] have generated an increasing number of studies focused on the thermally induced emissivity variation [6,7].

Light manipulation in the infrared wavelength range is a challenging strategy for several applications as energy harvesting, thermal radiation control [8] as well as IR sensing [9]. VO_2 thin films are also utilized for tunable and reconfigurable metamaterials in infrared wavelengths in thin film [6,10], multilayers [11] and metamaterial gold-VO_2 structures [12]. A hybrid VO_2/Au grating onto hBN/graphene/hBN heterostructures displayed bi-tunable absorption and transmission features [13].

The thermal hysteresis loop prevalent in phase transition processes has attracted increasing attention, and it was found to be affected by several factors such as the film deposition temperature [14], the wavelength range [15], the choice of suitable substrate [16,17], the use of metallic content [18] as well as the size of metallic phase domains [19]. Specifically, in [15] the hysteresis loop was investigated in both front and rear configuration, i.e. infrared radiation coming from the VO_2 layer and substrate, respectively and was found to be considerably different in the two configurations. The thermal hysteresis was also investigated for thin films with different thicknesses showing a clear dependence of the transition temperature and the width of the hysteresis loop on the film thickness and on the size of the crystallites [14]. The hysteresis loop was also characterized across different wavelength ranges and it was shown that some wavelengths allow large transmittance variation in contrast to other wavelengths, where the tunability was extremely reduced [18]. Critical temperature range was also discovered to depend on the operation wavelength, and it was attributed to the size of the metallic clusters created during phase transition [16]. In further investigations, doping is proven to affect and modify the hysteresis loop. For example, both the critical phase transition temperature and the hysteresis width were modified by doping VO_2 nanoparticles with Ti and F [17]. All of the investigated methods provide an array of parameters that allow the control of the phase transition characteristics such as smoothing temperature gradient, reducing hysteresis loop width, and varying the critical temperature. Thus, the obtained results in these lines of research are pivotal tools for designing, improving and customizing the performance of thermally tunable devices based on VO_2 thin films.

In this work we investigate, both theoretically and experimentally, the dynamic tuning of infrared emission from a single VO_2 thin film on sapphire substrate in the 3.3-5.1 μm wavelength range [20,21]. Within this wavelength range, we employed a highly emissive object placed below the sample to show different emission features arising at different heating/cooling rates. We first evaluate and address the effects of the different contributions to the overall IR radiation and investigate the critical role of VO_2 as the active material for thermal emission tuning [22]. Moreover, in our experiments, we observed different features for the hysteresis loop emphasizing the role of heating/cooling rate on emittance. Heating rate emerges as a promising parameter contributing to the resulting spectral features such as emittance or reflectance therefore could play important role in future device designs based on phase-change materials such as VO_2 thin films.

In the following, we first introduce the device under investigation and describe the IR thermographic experimental setup. Then, we experimentally demonstrate the variability of hysteresis loop obtainable for the given device under identical experimental configurations, while only modifying the heating/cooling rate. In order to provide better understanding of observed phenomenon, we develop a detailed numerical analysis and theoretical explanation using a homogenization technique in which VO_2 layer is modelled as a metamaterial with an effective dielectric constant. The agreement between our experimental findings and numerical simulations reveals that the process of metallization can be modeled as a binary system where inclusion aspect ratio is modulated by the heating rate.

Optics EXPRESS

2. Experimental

The VO_2 thin film (80 nm) was deposited on c-plane sapphire substrate using pulsed-laser-deposition (PLD) in 5 mTorr O_2 environment at 550°C substrate temperature, while the PLD laser energy was set at 321 mJ with 5 Hz pulse frequency. The same 5 mTorr O_2 environment was employed for a post-deposition annealing at 550°C for 30 mins.

Following the ASTM E1933-99a standard method in the contact-free configuration [23], the IR emissive properties of the VO_2 film has been investigated by infrared thermographic technique [24]. A reference material with known emissivity (thin layer of graphite paint [8]) is employed in order to retrieve the effective relative emissivity of the investigated sample. The measurements on the VO_2 film have been carried out by recording thermographic images for increasing temperature of the heating plate and finally cooling it down. Different heating/cooling rates are investigated, ranging from 1°C/s to 1°C/min in order to highlight the effect of temperature temporal dynamic on phase transition process.

The experimental apparatus as well as the sample geometry are schematically depicted in Fig. 1. The sample is placed onto a temperature-controlled aluminum stage. Above the heater, two distinct layers of graphite paint (Bonderite L-GP 386 Acheson) characterized by a well-known emissivity value [25] are deposited under and next to sample, respectively. Actual temperature evolution was monitored using two control thermocouples placed in contact with the reference graphite paint, and the sample, respectively. A stabilizer power supply was employed to avoid undesired oscillations in the heating current. The main axis of the IR camera, placed in front of the heating stage, was intentionally set slightly tilted to avoid detection of the spurious IR signal. Although the IR camera is working in the 3.3-5.1 micron wavelength range, ambient radiation was experimentally avoided using shields all around the experiment area. Furthermore, the IR camera software also requires to set the background temperature, so that IR radiation contribution to the measured signal arising from the spurious environmental radiation can be compensated.

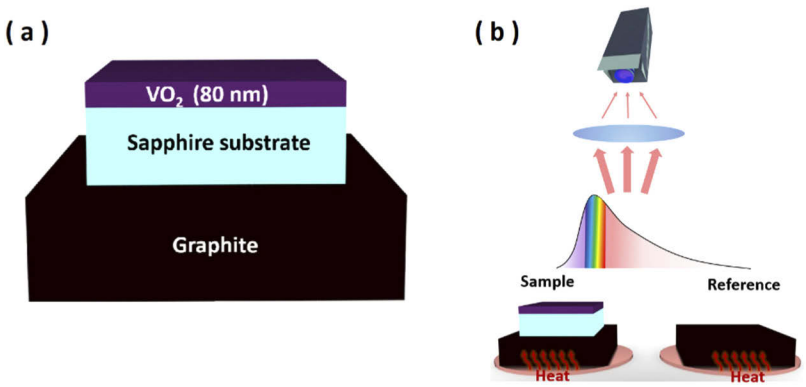

Fig. 1. (a) Schematic sketch of the sample on a high emissivity reference paint (black-body-like) source, and (b) schematic representation of the experimental setup.

The spectral intensity of the emitted IR radiation was investigated using a CEDIP Jade MWIR camera operating in the mid-infrared wavelength range (3.5-5.1 microns) completed by a manual focusing lens with a focal length of 25 mm. The thermographic imaging system is composed by a focal plane array of 320×240-pixel InSb detectors, with a lateral dimension (pixel pitch) of 30 μm. The minimum temperature difference resolvable by the IR camera, i.e. the noise equivalent temperature difference (NETD) is 25 mK at 300 K. The measurements have been carried out by recording thermographic images for increasing temperature of the heating plate, between 45°C and 85°C. After each measurement the thermographic images were processed using a software

Optics EXPRESS

developed in MATLAB environment where the image pixels corresponding to either sample or reference surface can be selected, to retrieve the average emitted IR radiation.

From experimental data the emitted VO_2 signals were normalized with respect to that emitted by the graphite reference sample and are reported using markers in Fig. 2, where theoretical fitting curves are shown with solid lines. In the panels of Fig. 2, red colors indicate the heating process while the blue lines correspond to the cooling branch. Furthermore, the typical hysteresis loop, intrinsically arising from the phase transition dynamics, is considerably visible, despite VO_2 its only 80 nm thick.

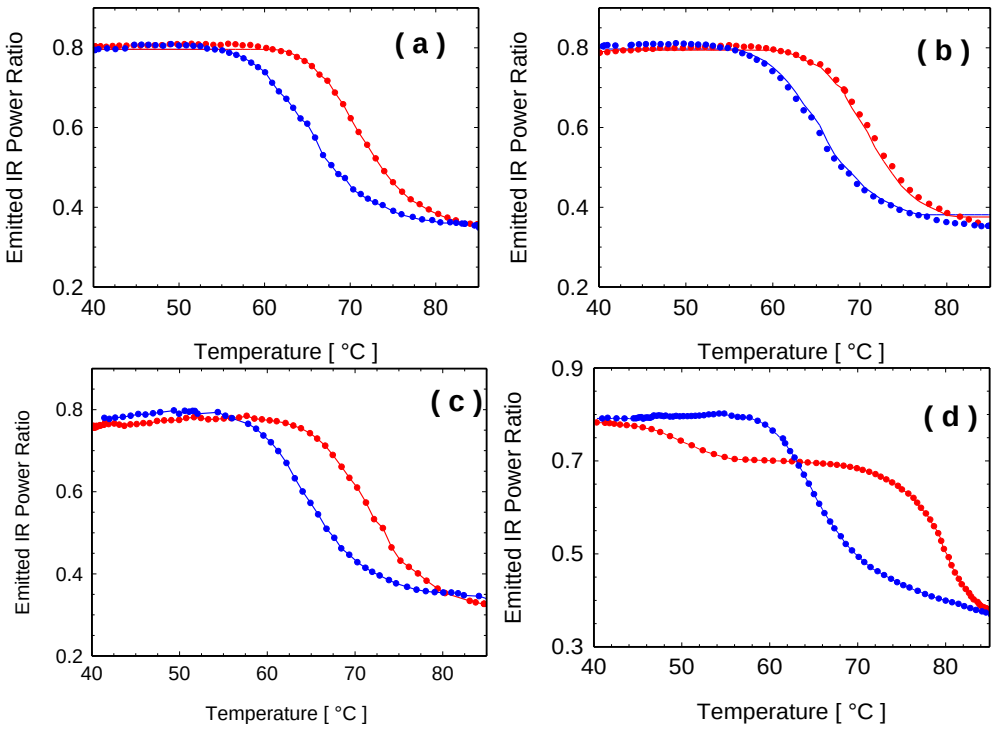

Fig. 2. Relative emitted power of the VO_2(80 nm)/sapphire/graphite system measured via infrared thermography technique in the 3.3-5.1 μm wavelength range. In alphabetic order, results for increasing heating (red curves) and cooling (blue curves) rates are displayed: (a) 1deg/60sec, (b) 1deg/30sec, (c) 1deg/15sec and (d) 1deg/1sec. Markers represent experimental data while continuous lines are the theoretically fit curves. Different depolarization factors are employed for simulations (see Table 1).

Table 1. Hysteresis loops main characteristics.

Heating/Cooling Rate	Transition Temperature [°C] $T_{heating}$, $T_{cooling}$	Width $T_{cooling}$ - $T_{heating}$ [°C]	Depolarization Factors Range L_β=L_γ
1°C/60s	65.2, 70.1	4.9	0
1°C/30s	64.4, 71.4	7.0	0.10-0.14
1°C/15s	63.5, 72.4	8.9	0.13-0.16
1°C/1s	64.5, 79.8	15.3	0.21-0.25

Below phase transition temperature, in the investigated wavelength range the sample is mostly transparent [26]. First of all, Fig. 2 infers that when the VO_2 structure is placed over high

Optics EXPRESS

emissive graphite surface, the infrared radiation arising from the VO_2/Sapphire/graphite system switches from high to low value as temperature is increased. Thus, it is possible to define a critical temperature (T_c), where the slope of the signal is maximum, with a large dynamic range of about 0.4. The IR radiation emitted from the graphite is initially transmitted from insulating VO_2. However, when the phase transition takes place, the metallic VO_2 progressively shields the contribution of the underlying black body. More interestingly, different panels of Fig. 2 also suggest that the overall system behaves differently if the sample is heated at low or high heating rate.

In the next section, we will analyze and discuss the different dynamics of phase transition and emissivity variation, correlate them to the metallic phase formation and interpret accordingly.

3. Discussion

Thermal emission from hot objects is governed by Planck's law, where an ideal black-body perfectly absorbs/emits over the entire electromagnetic spectrum for all incident angles. Once real bodies are considered, the ability to radiate heat is compared to a black-body [27] and designate the relative thermal emissivity.

Starting from experimental data we retrieved an effective average emissivity of the system which encompasses both the VO_2 device and the underlying heat source. The resulting effective relative emissivity of the system in the camera wavelength range $\langle \varepsilon_{eff}(T) \rangle$ is obtained as the ratio of the emitted signal from sample, $S_{sample}(T)$, normalized using the reference, black-body, graphite paint ($S_{ref}(T)$) :

$$\langle \varepsilon_{eff}(T) \rangle = \frac{S_{\text{sample}}(T)}{S_{\text{ref}}(T)} = \frac{\int_{\lambda_{\min}}^{\lambda_{\max}} \left(\frac{2hc^2 \varepsilon_{eff}(\lambda,T)}{\lambda^5 \left(e^{\left(\frac{hc}{k_B \lambda T}\right)} - 1 \right)} \right) d\lambda}{\int_{\lambda\,\min}^{\lambda\,\max} \left(\frac{2hc^2 \varepsilon_{\text{graphite}}(\lambda,T)}{\lambda^5 \left(e^{\left(k_B \lambda T\right)} \right)_{-1}} \right) d\lambda} \tag{1}$$

In Eq. (1), $\frac{2hc^2}{\lambda^5 \left(e^{\left(\frac{hc}{k_B \lambda T}\right)} - 1 \right)}$ represents the power spectral density per unit area radiated by a perfect black-body, h is the Planck's constant, c is the speed of light in vacuum, k_B is the Boltzmann constant, and λ_{min} and λ_{max} delimitate lower and upper limit of the camera operational wavelength range [28].

For experimental data interpretation the VO_2 film is modeled as a metamaterial for a temperature range close to its critical temperature, being its thickness thin if compared to the wavelengths of interest [29,30]. As the filling factor is increased from f=0 (full semiconductor state) to f=1 (full metallic state), the metallic phase is microscopically described as ellipsoidal nanoscale inclusions into a semiconductor matrix, eventually giving rise to percolation behaviour [31]. The inclusions and hence their temperature evolution can be described using Maxwell Garnett mixing formulas for ellipsoidal inclusions into a matrix, as reported in Ref. [32]. The electrical permittivity components along inclusions' main axes, i.e. α− β− and γ− axes, are calculated using [33]:

$$\varepsilon_{eff,j} = \varepsilon_S + f \frac{\varepsilon_S(\varepsilon_M - \varepsilon_S)}{\varepsilon_S + (1-f)L_j(\varepsilon_M - \varepsilon_S)}; \tag{2}$$

where, ε_S and ε_M represent the relative permittivities of the host semiconducting matrix (VO_2 below T_c) and the metallic inclusions (VO_2 above T_c), respectively. The inclusions content is specified by the filling factor, f, while the parameters L_j (j=α, β and γ) represent the depolarization

Optics EXPRESS

factors [32] (always fulfilling the requirement $L_\alpha+L_\beta+L_\gamma=1$). The refractive index values of VO_2 in the semiconductor and metallic states were taken from Ref. [34]. According to this model, both shape and orientation of ellipsoidal inclusions with respect to coordinate axes are described by the three depolarization factors. In Fig. 3 we show some possible combinations for depolarization factors for uniaxial inclusions ($L_\beta=L_\gamma$) ranging from oblate ($L_\alpha=1$, $L_\beta=L_\gamma=0$) to elongate ($L_\alpha=0$, $L_\beta=L_\gamma=0.5$) limits. Following the calculation of the directional dielectric permittivity components vs the filling factor, refractive indices and extinction coefficients along the corresponding axes are retrieved using the given the relations $Re(\varepsilon) = n^2 - k^2$ and $Im(\varepsilon) = 2nk$.

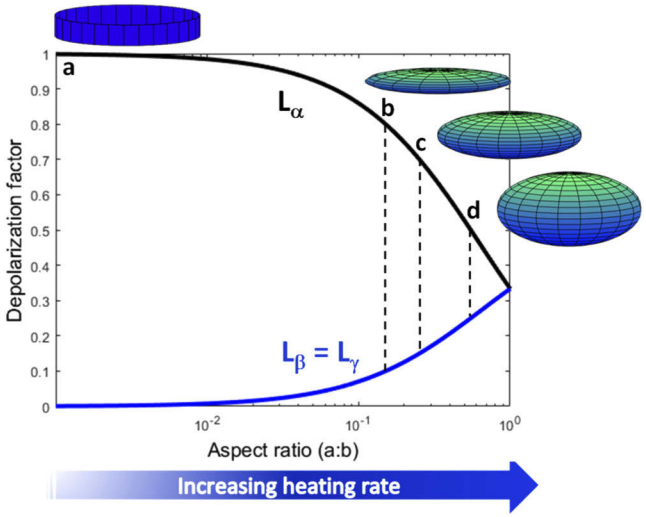

Fig. 3. Depolarization factors, L_α L_β and L_γ, for uniaxial ellipsoids (L_β=L_γ). Letters on the graphs (a,b,c,d) designate the average ellipsoids aspect ratio employed to retrieve the fitting curves in the graphs of Fig. 2. From left to right heating/cooling rate is increasing.

Using transfer matrix method (TMM) techniques, we simulated an equivalent layer, having effective medium properties calculated by Eq. (2). Layer's optical transmittance and reflectance on an axis normal to the film surface, $T(\omega)$ and $R(\omega)$, were calculated at increasing filling factor values. In accordance with energy conservation, for lossy media, the real absorbance can be calculated according to Kirchoff's first law $A(\omega) = 1-R(\omega)-T(\omega)$ while thermal emitted radiation is given by $\varepsilon(\omega)=A(\omega)$ [35,36].

According to experimental configuration shown in Fig. 1, if the heater reflectivity is negligible, as is in the present case, the infrared signal ratio, $\langle \varepsilon_{eff}(T) \rangle = \frac{S_{sample(T)}}{S_{ref(T)}}$, detected by the infrared camera can be described as follows:

$$\varepsilon_{eff}(\lambda,\ T) = \varepsilon_{VO2}(\lambda,\ T) + \varepsilon_{heater} \cdot T_{VO2}(\lambda,\ T); \tag{3}$$

The first contribution is given by the infrared radiation emitted by the VO_2 film ($\varepsilon_{VO2}(\lambda,\ T)$) over sapphire substrate. The second contribution is due to the infrared radiation emitted by the heater, ε_{heater}, (black-body -like graphite paint) and then transmitted by the VO_2 film ($T_{VO2}(\lambda,\ T)$). If the infrared reflectance of the heater is significant, the IR radiation reflected from bottom interface and then forward transmission through the VO_2 can also be considered [24]. Once the spectral features are retrieved via TMM method, their contributions (see Eq. (3)) to the effective emissivity can be calculated and then incorporated in the Planck formula (Eq. (1)), for the different temperature dynamics, respectively.

It is evident from experimental curves of Fig. 2 that the signal arising from the graphite heat source is strongly attenuated as the temperature increases beyond T_c, since the VO_2 film becomes

Optics EXPRESS

progressively opaque. Moreover, a non-negligible role is played by the rate of temperature increase/decrease. As heating/cooling rate is increased, the hysteresis loop appears to broaden, and its shape is also slightly altered. In order to fit the experimental variations observed in the hysteretic loop shape and width, we provide the following interpretation; by looking at Fig. 3, point a, i.e. the lowest heating/cooling rate, where temperature is increased at lowest rate, 1°C/60sec, the VO_2 film has enough time to thermalize and heat flows across the entire film thickness. Thanks to the longer time step, between two consecutive temperature values, heat distribution gets laterally uniform. Under these circumstances, the inclusions of metallic phase can be modeled as disk-like inclusions, thus depolarization factors are fixed to $L_\alpha=1$, $L_\beta=L_\gamma=0$, i.e. at the oblate side of the graph in Fig. 3. [37,39]. Contrarily, when heating process gets faster, another scenario for metallic inclusions is assumed to unfold. Specifically, we modified the depolarization factor values and progressively decrease L_α (along disk thickness) and increase $L_\beta = L_\gamma$ (along inclusions cross section). The resulting inclusions shape is gradually modified from disk to an oblate ellipsoidal shape: disk thickness is increased while disk diameter shrinks. It's worth noting that we restricted our investigation up to the spherical shape of ellipsoids ($L_\alpha=L_\beta=L_\gamma=1/3$). Indeed, the elongate side of graph in Fig. 3, i.e. prolate (cylindrical) inclusion shape, would require $L_\alpha=0$ that is not consistent with the small VO_2 film thickness (80 nm). As a result, the dielectric constant anisotropy is attenuated when going from the oblate extreme to the spherical inclusion shape, thus modifying refractive index and extinction coefficient of the resulting effective medium.

The fitting curves reported in Fig. 2 as solid lines, have been obtained by applying a least squares fitting procedure to the infrared signal ratio as defined in Eq. (3). Both filling factor and depolarization factors are fitting parameters and are modified during phase transition as a function of the temperature, in order to retrieve the film dielectric constant, during the heating and cooling processes, respectively. Both filling and depolarization factors are functions of temperature and of the heating/cooling rate. The filling factor takes into account the relative quantity of (increasing/decreasing) metallic inclusions while the depolarization factors behavior takes into account a progressive change in the ellipsoidal inclusions' shape. The combination of both these parameters results in effective index media exhibiting different slopes at different heating/cooling regimes. As an example, in Fig. 4(a) and Fig. 4(b) we display the filling factor, f, and depolarization factors, $L_\beta=L_\gamma$, vs temperature, obtained for the fitting curve reported in Fig. 2(b), i.e. corresponding to a heating/cooling rate of 1deg/30sec.

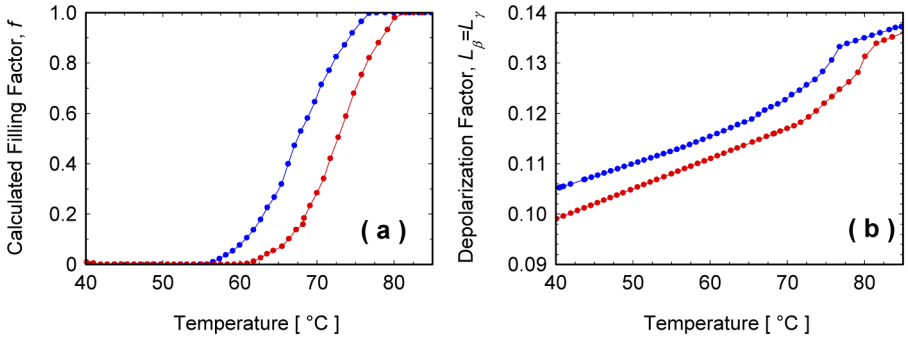

Fig. 4. (a) Filling factor and (b) depolarization factors, $L_\beta=L_\gamma$, as retrieved for the fitting procedure of experimental measurements at heating/cooling rate 1deg/30sec (corresponding to Fig. 2(b)). Different results are obtained for heating (red curves) and cooling (blue curves) branches, respectively.

As a further investigation, we calculated the derivative of experimental curves shown in Fig. 2 in order to highlight how the phase transition effective critical temperature T_c can be engineered

Optics EXPRESS

by varying heating/cooling rate. In Fig. 5 the slope of experimental signals vs temperature is shown, and the critical temperature can be extracted from their minima during heating and cooling cycles, respectively. The asymmetry between heating and cooling curves is evidenced by the two minima of the derivative curves. Furthermore, from this graph it is clear that an accurate control of the heating/cooling rate would allow the tuning and managing of hysteresis loops' width. Another important point observable from experimental findings is that the heating cycle corresponding to the highest heating/cooling rate (1°C/s) follows different path whit respect to other curves. On one hand we expect that high heating/cooling rate could result in a shift in the T_c since we expect an offset between the temperature of the heater and the temperature of the VO_2 related to the thermal conductivity of both the sapphire and the VO_2 film. On the other hand, the experimentally measured nested (or twisted) loop (see Fig. 2(d)) suggests that during the phase transition, the response time of the system with respect to the heating/cooling rate depends on the behavior of the phase inclusions parameters such as filling factor and inclusion aspect ratios. Indeed, the thermal conductivity of the VO_2 film also switches from semiconductor to metallic phase [40] and our measurements reveal that it might experience a complex behavior during the phase transition process due to the coexistence of the two phases. This result suggests further investigation of the thermal conductivity properties of the VO_2 film during the phase transition which is beyond the scope of this work.

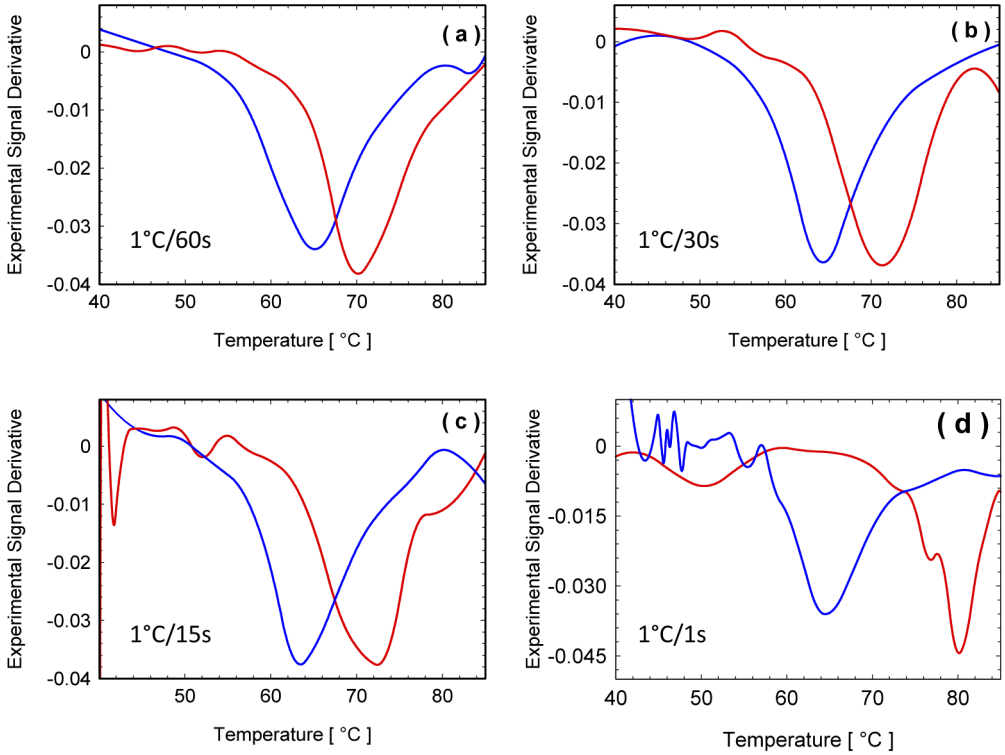

Fig. 5. Derivative of emitted IR power ratio vs temperature, for different heating/cooling rates. The results for increasing heating (red curves) and cooling (blue curves) rates are displayed when the rate is equal to (a) 1deg/60sec, (b) 1deg/30sec, (c) 1deg/15sec and (d) 1deg/1sec.

To get a more intriguing sight at the experimental results, we selected the two heating branches corresponding to the two extremes, i.e. the slowest (1°C/60sec) and the highest (1°C/s) cooling rate, as reported in Fig. 6. In Figs. 7, we show the IR thermographic images corresponding to the

Optics EXPRESS

different temperature highlighted with vertical black lines in Fig. 6. It is worth noting that, for the extreme temperature points 40°C and 85°C, the IR signals reach comparable digital levels, for both heating rates. Similar experimental results are observed when comparing thermographic images obtained at the nominal critical transition temperature for VO_2 (68°C), representing the point where the two experimental curves intersect. However, the potential of the heating rate as a parameter to tune the IR emissivity of the VO_2 based device is fully evidenced when $T < T_c$ or $T > T_c$. Here, we observe that when $T < T_c$ (Fig. 7, temperature 63°C) the IR emitted radiation is higher for the case of slower heating rate (left column) with respect to faster heating rate (right column). Interestingly, the opposite behavior is observed when $T > T_c$ (Fig. 7, temperature 77°C) where the higher IR emitted radiation is obtained for the faster heating rate (right column). The observed feature might have interesting applications for thermal camouflage devices, i.e. the emissivity of a source could be tuned by modulating the temperature of an external VO_2 coated shield around its transition temperature at the proper heating/cooling rate.

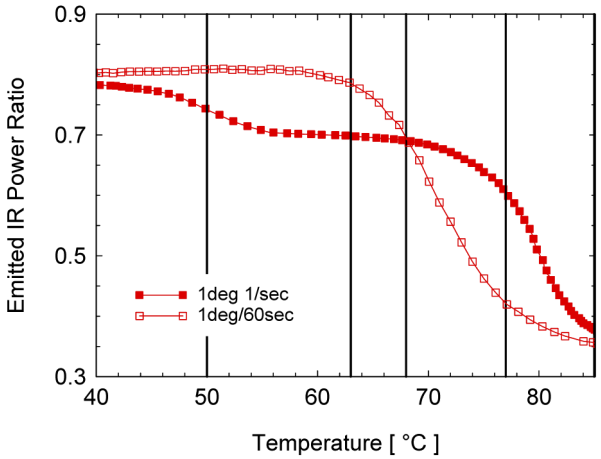

Fig. 6. Relative emitted power of the VO_2-(80 nm)/sapphire/graphite system measured via infrared thermography technique in the 3.3-5.1 μm wavelength range. Comparison between the lowest (1deg/60sec) and highest (1deg/1sec) heating rates are displayed.

The experimental results show that the infrared emission of the resulting effective layer can be suppressed on demand by a sub-wavelength VO_2 thin film. Furthermore, the obtained experimental fitting curves suggest that tuning the rate of temperature variation might be used as a further parameter to control the phase transition for smoothing gradient, modifying hysteresis loop width, and eventually affecting the effective critical temperature. The main features of the hysteresis loops obtained under different heating/cooling rate conditions are summarized in Table 1.

Optics EXPRESS

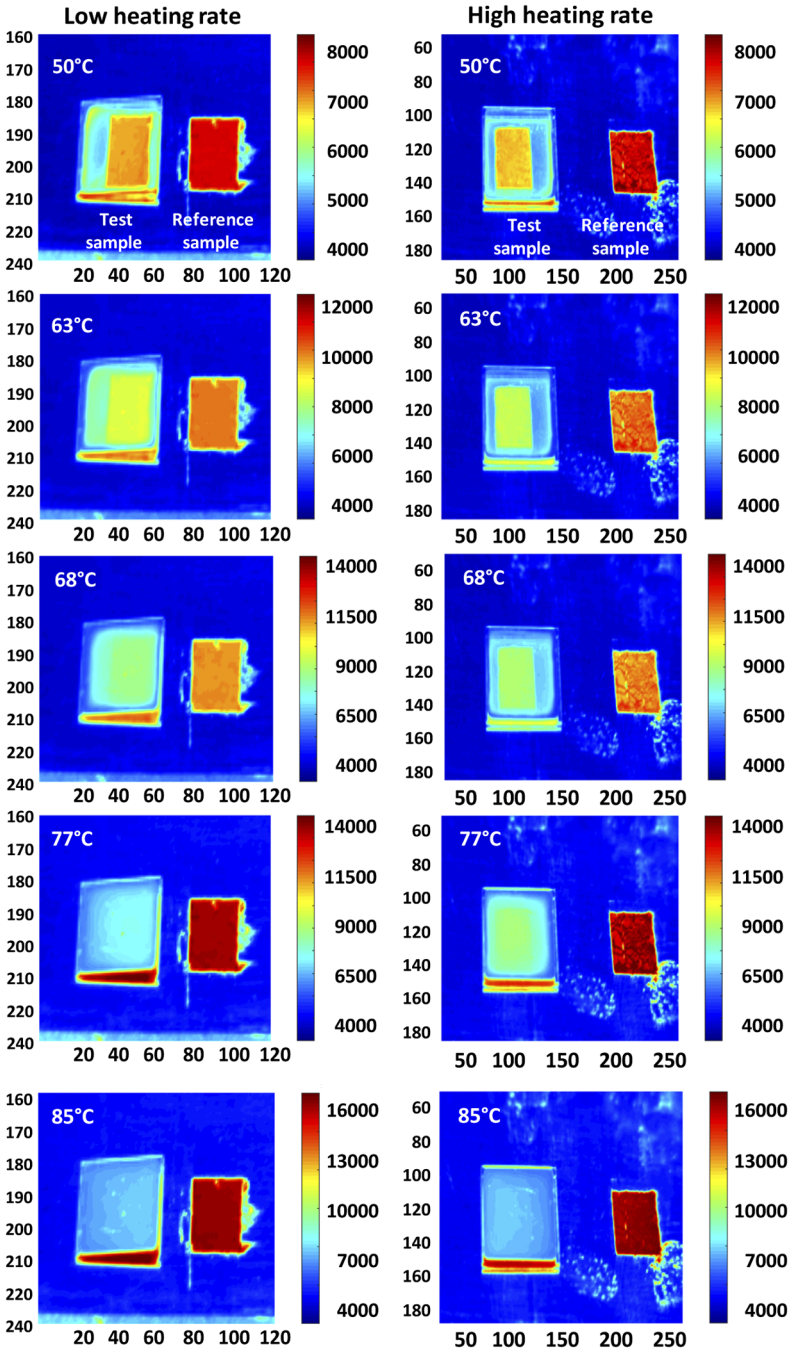

Fig. 7. . IR thermographic images obtained from VO_2(80 nm)/sapphire/graphite system measured in the 3.3-5.1 μm wavelength range under different heating regime: lowest heating rate (left column) and highest heating rate (right column), respectively.

Optics EXPRESS

4. Conclusions

We investigated the possibility of tuning IR radiation from a device consisting of a thin VO_2 thermochromic film, using different heating/cooling rate. Beyond many explored factors such as film deposition temperature, different substrates, the wavelength range and metallic doping, the rate of heating/cooling process can also affect the dynamic of the phase transition. Increasing or decreasing temperature at different rates highlighted the on-demand infrared emission features which were successfully described by effective medium theory. These results highlight the significance of heating/cooling rates as tuning parameters for the optical response of VO_2. These findings can be useful for microscopic sensing of phase change dynamics through macroscopic optical response of phase change materials. Moreover, applying our findings to optical devices can open new avenues in search of actively tunable infrared photonic systems with the heating/cooling rate as an additional engineerable parameter.

As a general feature, the characteristic phases coexistence, represented by the hysteresis loop itself, enables high tunability of electrical, optical and emissive properties. Among the several applications where the hysteresis loop is of fundamental importance, the most appealing is the realization of radiative thermal logic elements and gates based on phase transition materials [41]. For such applications, the phase transition region is shifted whether VO_2 elements are heated or cooled. Furthermore, depending on the way the logic gates are employed, electrical heating or laser pumping for instance, also temperature operation range will be slightly modified. Taming and tuning of the hysteresis loop can be an important tool for device designing and optimization.

Funding

Sapienza Università di Roma (Bando Professori Visitatori 2018, Progetti di Ateneo 2017); Director, Office of Science, Office of Basic Energy Sciences, Materials Sciences and Engineering Division, of the U.S. Department of Energy (DE-AC02-05CH11231); Office of Naval Research (ONR-YIP N00014-17-1-2425).

Acknowledgments

K.A. acknowledges support from the Office of Naval Research Young Investigator Program (ONR-YIP) Award (N00014-17-1-2425). K.A. and M.C.L. also acknowledge the support from University La Sapienza for the Visiting Professor Program 2018 (Bando Professori Visitatori 2018) as well as for Sapienza Research Program 2017 (Progetti di Ateneo 2017). K.T. and J.W were supported by the Director, Office of Science, Office of Basic Energy Sciences, Materials Sciences and Engineering Division, of the U.S. Department of Energy under Contract No. DE-AC02-05CH11231.

Disclosures

The author(s) declare no competing interests.

References

1. H. Liu, J. Lu, and X.R. Wang, "Metamaterials based on the phase transition of VO_2," Nanotechnology **29**(2), 024002 (2018).
2. F. Gervais and W. Kress, "Lattice dynamics of oxides with rutile structure and instabilities at the metal-semiconductor phase transitions of NbO_2 and VO_2," Phys. Rev. B **31**(8), 4809–4814 (1985).
3. M. Nakahira, S. Horiuchi, and H. Ooshima, "Low-Temperature Phase Transition of Vanadium Sesquioxide," J. Appl. Phys. **41**(2), 836–838 (1970).
4. Z. Liu, B. Banar, S. Butun, H. Kocer, K. Wang, J. Scheuer, J. Wu, and K. Aydin, "Dynamic infrared thin-film absorbers with tunable absorption intensity based on VO_2 phase transition," Opt. Mater. Express **8**(8), 2151–2158 (2018).

Optics EXPRESS

5. Y. Zhao, C. Chen, X. Pan, Y. Zhu, M. Holtz, A. Bernussi, and Z. Fan, "Tuning the properties of VO_2 thin films through growth temperature for infrared and terahertz modulation application," J. Appl. Phys. **114**(11), 113509 (2013).
6. K. Liu, S. Lee, S. Yang, O. Delaire, and J. Wu, "Recent progress on physics and applications of vanadium dioxide," Mater. Today **21**(8), 875–896 (2018).
7. E. Petronijević and C. Sibilia, "Thin films of phase change materials for light control of metamaterials in the optical and infrared spectral domain," Opt. Quantum Electron. **52**(2), 110 (2020).
8. M.C. Larciprete, S. Paoloni, N. Orazi, F. Mercuri, M. Orth, Y. Gloy, M. Centini, R. Li Voti, and C. Sibilia, "Infrared emissivity characterization of carbon nanotubes dispersed poly (ethylene terephthalate) fibers," Int. J. Therm. Sci. **146**, 106109 (2019).
9. G. Deng, X. Song, S. A. Dereshgi, H. Xu, and K. Aydin, "Tunable multi-wavelength absorption in mid-IR region based on a hybrid patterned graphene-hBN structure," Opt. Express **27**(16), 23576–23584 (2019).
10. H. Kocer, S. Butun, E. Palacios, Z. Liu, S. Tongay, D. Fu, K. Wang, J. Wu, and K. Aydin, "Intensity tunable infrared broadband absorbers based on VO_2 phase transition using planar layered thin films," Sci. Rep. **5**(1), 1–5 (2015).
11. R. Li Voti, M.C. Larciprete, G. Leahu, C. Sibilia, and M. Bertolotti, "Optical response of multilayer thermochromic VO_2-based structures," J. Nanophotonics **6**(1), 061601 (2012).
12. H. Kocer, S. Butun, B. Banar, K. Wang, S. Tongay, J. Wu, and K. Aydin, "Thermal tuning of infrared resonant absorbers based on hybrid gold-VO_2 nanostructures," Appl. Phys. Lett. **106**(16), 161104 (2015).
13. H. Hajian, A. Ghobadi, A.E. Serebryannikov, B. Butun, G.A.E. Vandenbosch, and E. Ozbay, "VO_2-hBN-graphene-based bi-functional metamaterial for mid-infrared bi-tunable asymmetric transmission and nearly perfect resonant absorption," J. Opt. Soc. Am. B **36**(6), 1607–1615 (2019).
14. J.A. Ramirez-Rincon, C.L. Gomez-Heredia, A. Corvisier, J. Ordonez-Miranda, T. Girardeau, F. Paumier, C. Champeaux, F. Dumas-Bouchiat, Y. Ezzahri, K. Joulain, O. Ares, and J.J. Alvarado-Gil, "Thermal hysteresis measurement of the VO_2 dielectric function for its metal-insulator transition by visible–IR ellipsometry," J. Appl. Phys. **124**(19), 195102 (2018).
15. G. Cesarini, G. Leahu, A. Belardini, M. Centini, R. Li Voti, and C. Sibilia, "Quantitative evaluation of emission properties and thermal hysteresis in the mid-infrared for a single thin film of vanadium dioxide on a silicon substrate," Int. J. Therm. Sci. **146**, 106061 (2019).
16. T. Cesca, C. Scian, E. Petronijevic, G. Leahu, R. Li Voti, G. Cesarini, R. Macaluso, M. Mosca, C. Sibilia, and G. Mattei, "Correlation between in-situ structural and optical characterizations of the semiconductor-to-metal phase transition of VO_2 thin films on sapphire," Nanoscale **12**(2), 851–863 (2020).
17. R. Li Voti, G. Leahu, M.C. Larciprete, C. Sibilia, and M. Bertolotti, "Photothermal Characterization of Thermochromic Materials for Tunable Thermal Devices," Int. J. Thermophys. **36**(5-6), 1004–1015 (2015).
18. M. Okada, A. Takeyama, and Y. Yamada, "Thermal hysteresis control of VO_2 (M) nanoparticles by Ti-F codoping," Nano-Struct. Nano-Objects **20**, 100395 (2019).
19. J. Liang, M. Hu, Q. Kan, X. Liang, X. Wang, G. Li, and H. Chen, "Infrared transition properties of vanadium dioxide thin films across semiconductor metal-transition," Rare Met. **30**(3), 247–251 (2011).
20. F. Mercuri, N. Orazi, S. Paoloni, C. Cicero, and U. Zammit, "Pulsed Thermography Applied to the Study of Cultural Heritage," Appl. Sci. **7**(10), 1010 (2017).
21. N. Orazi, F. Mercuri, U. Zammit, S. Paoloni, M. Marinelli, A. Giuffredi, and C.S. Salerno, "Thermographic analysis of bronze sculptures," Stud. Conserv. **61**(4), 236–244 (2016).
22. M. C. Larciprete, M. Centini, S. Paoloni, I. Fratoddi, S. A. Dereshgi, K. Tang, J. Wu, and K. Aydin, "Adaptive tuning of infrared emission using VO_2 thin films," Sci. Rep. **10**(1), 11544 (2020).
23. ASTM E1933-99a, "*Standard Test Methods for Measuring and Compensating for Emissivity Using Infrared Imaging Radiometers*", American Society for Testing and Materials International, West Conshohocken, PA (1999).
24. F. Mercuri, R. Gnoli, S. Paoloni, N. Orazi, C. Cicero, U. Zammit, M. Marinelli, and F. Scudieri, "Hidden text detection by infrared thermography," Restaurator **34**(3), 195–211 (2013).
25. M.C. Larciprete, S. Paoloni, R. Li Voti, Y.S. Gloy, and C. Sibilia, "Infrared radiation characterization of several stainless steel textiles in the 3.5–5.1 μm infrared range," Int. J. Therm. Sci. **132**, 168–173 (2018).
26. M. Schubert, T.E. Tiwald, and C.M. Herzinger, "Infrared dielectric anisotropy and phonon modes of sapphire," Phys. Rev. B **61**(12), 8187–8201 (2000).
27. C.M. Cornelius and J.P. Dowling, "Modification of Planck blackbody radiation by photonic band-gap structures," Phys. Rev. A **59**(6), 4736–4746 (1999).
28. Z. Xu, Q. Li, K. Du, S. Long, Y. Yang, X. Cao, H. Luo, H. Zhu, P. Ghosh, W. Shen, and M. Qiu, "Spatially Resolved Dynamically Reconfigurable Multilevel Control of Thermal Emission," Laser Photonics Rev. **14**(1), 1900162 (2020).
29. S.A. Dönges, O. Khatib, B.T. O'Callahan, J.M. Atkin, J. H. Park, D. Cobden, and M.B. Raschke, "Ultrafast nanoimaging of the photoinduced phase transition dynamics in VO_2," Nano Lett. **16**(5), 3029–3035 (2016).
30. B.T. O'Callahan, A.C. Jones, J. Hyung Park, D.H. Cobden, J.M. Atkin, and M.B. Raschke, "Inhomogeneity of the ultrafast insulator-to-metal transition dynamics of VO_2," Nat. Commun. **6**(1), 6849 (2015).
31. K.H. Matlack, M. Serra-Garcia, A. Palermo, S.D. Huber, and C. Daraio, "Designing perturbative metamaterials from discrete models," Nat. Mater. **17**(4), 323–328 (2018).
32. A. Sihvola, "Homogenization principles and effect of mixing on dielectric behaviour," Photonics Nanostruct **11**(4), 364–373 (2013).

Optics EXPRESS

33. M.C. Larciprete, M. Centini, R. Li Voti, and C. Sibilia, "Selective and tunable thermal emission in metamaterials composed of oriented polar inclusions," J. Opt. Soc. Am. B **34**(7), 1459–1464 (2017).
34. H. Kakiuvhida, P. Jin, S. Nakao, and M. Tazawa, "Optical Properties of Vanadium Dioxide Film during Semiconductive–Metallic Phase Transition," Jpn. J. Appl. Phys., Part 1 **46**(5), L113–L116 (2007).
35. J.W. Salisbury, A. Wald, and D.M. D'Aria, "Thermal-infrared remote sensing and Kirchhoff's law: 1. Laboratory measurements," J. Geophys. Res.: Solid Earth **99**(B6), 11897–11911 (1994).
36. L. Xiao, H. Ma, J. Liu, W. Zhao, Y. Jia, Q. Zhao, K. Liu, Y. Wu, Y. Wei, S. Fan, and K. Jiang, "Fast adaptive thermal camouflage based on flexible VO_2/graphene/CNT thin films," Nano Lett. **15**(12), 8365–8370 (2015).
37. M.M. Qazilbash, M. Brehm, G.O. Andreev, A. Frenzel, P.-C. Ho, B.-G. Chae, B.-J. Kim, S. Jin Yun, H.-T. Kim, A.V. Balatsky, O.G. Shpyrko, M.B. Maple, F. Keilmann, and D.N. Basov, "Infrared spectroscopy and nano-imaging of the insulator-to-metal transition in vanadium dioxide," Phys. Rev. B **79**(7), 075107 (2009).
38. H.S. Choi, J.S. Ahn, J.H. Jung, T.W. Noh, and D.H. Kim, "Mid-infrared properties of a VO_2 film near the metal-insulator transition," Phys. Rev. B **54**(7), 4621–4628 (1996).
39. J.A. Ramirez-Rincon, C.L. Gomez-Heredia, A. Corvisier, J. Ordonez-Miranda, T. Girardeau, F. Paumier, C. Champeaux, F. Dumas-Bouchiat, Y. Ezzahri, K. Joulian, O. Ares, and J.J. Alvarado-Gil, "Thermal hysteresis measurement of the VO_2 dielectric function for its metal-insulator transition by visible–IR ellipsometry," J. Appl. Phys. **124**(19), 195102 (2018).
40. D.-W. Oh, C. Ko, S. Ramanathan, and D.G. Cahill, "Thermal conductivity and dynamic heat capacity across the metal-insulator transition in thin film VO_2," Appl. Phys. Lett. **96**(15), 151906 (2010).
41. C. Kathmann, M. Reina, R. Messina, P. Ben-Abdallah, and S.-A. Biehs, "Scalable radiative thermal logic gates based on nanoparticle networks," Sci. Rep. **10**(1), 3596 (2020).